THE JOURNAL OF PHYSICAL CHEMISTRY Letters

Letter

pubs.acs.org/JPCL

Phonon-Enabled Carrier Transport of Localized States at Non-Polar Semiconductor Surfaces: A First-Principles-Based Prediction

Dong Han,[†,‡,§] Junhyeok Bang,[*,∥] Weiyu Xie,[†] Vincent Meunier,[†] and ShengBai Zhang[*,†]

[†]Department of Physics, Applied Physics, and Astronomy, Rensselaer Polytechnic Institute, Troy, New York 12180, United States

[‡]State Key Laboratory of Luminescence and Applications, Changchun Institute of Optics, Fine Mechanics and Physics, Chinese Academy of Sciences, Changchun 130033, China

[§]State Key Laboratory on Integrated Optoelectronics, College of Electronic Science and Engineering, Jilin University, Changchun 130012, China

[∥]Spin Engineering Physics Team, Korea Basic Science Institute (KBSI), Daejeon 305-806, Republic of Korea

Supporting Information

ABSTRACT: Electron−phonon coupling can hamper carrier transport either by scattering or by the formation of mass-enhanced polarons. Here, we use time-dependent density functional theory-molecular dynamics simulations to show that phonons can also promote the transport of excited carriers. Using nonpolar InAs (110) surface as an example, we identify phonon-mediated coupling between electronic states close in energy as the origin for the enhanced transport. In particular, the coupling causes localized excitons in the resonant surface states to propagate into bulk with velocities as high as 10^6 cm/s. The theory also predicts temperature enhanced carrier transport, which may be observable in ultrathin nanostructures.

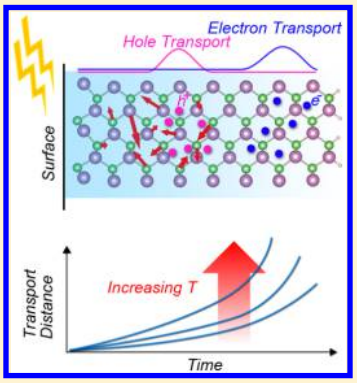

Controlling carrier transport is key to electronic device applications. As the size of devices continues to shrink to the sub-100-nm regime and molecular electronics are being demonstrated in laboratories,[1−4] study of quantum transport is becoming increasingly important. A number of interesting physical phenomena such as resonant tunneling, quantized conductance, and strong and weak localizations have been observed in a number of material systems.[5−8] At the same time, theoretical modeling based on first-principles calculations has been repeatedly shown central in providing crucial insights into transport phenomena both in the ballistic and diffusive regimes.[9−13] However, most of the first-principles studies thus far assume that the systems are prepared in their electronic ground state. Such an assumption is inadequate for the transport of excited carriers, which can be critical to the efficiency of optoelectronic devices. Moreover, charge carriers are often excited into empty energy levels within a very short period of time. As such, their dynamics take place far away from equilibrium,[14,15] for which current first-principles approaches are noticeably lacking.

Excited carrier transport is usually investigated in the framework of model systems or semiclassical theory. For example, the ensemble Monte Carlo modeling of the Boltzmann transport equation has been used to study the high energy carrier dynamics in Si, GaAs, and InAs.[16,17] In the semiclassical theory, excited carriers are treated as point charges endowed with an effective mass[18−22] and the systems are often treated under steady-state conditions. Although such studies have been successful in explaining the diffusion of excited carriers,[22−24] the semiclassical treatment is only an approximation to the actual processes. As depicted in Figure 1, an initial above-band-edge excitation of energy $h\nu_0$ at $t = 0$ first relaxes by an amount $\Delta E = \Delta E_e + \Delta E_h$ within time $t_0 < t < t_1$ to the band-edge states, where ΔE_e and ΔE_h are the energy

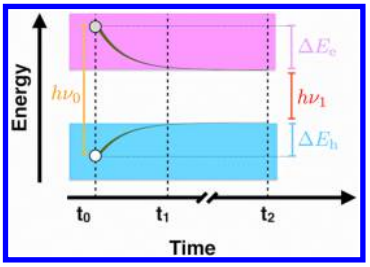

Figure 1. (Color online) Schematic illustration of time evolution of an above-band-edge excitation. The initial excitation at $t = t_0$ has an energy $h\nu_0$, as provided by a laser. It is lowered through excited electron and hole relaxation by an energy ΔE_e and ΔE_h, respectively, at $t = t_1$. After another characteristic time $t = t_2$, the electron−hole pair recombines, emitting a photon of energy $h\nu_1$.

Received: July 21, 2016
Accepted: August 23, 2016
Published: August 23, 2016

DOI: 10.1021/acs.jpclett.6b01608
J. Phys. Chem. Lett. 2016, 7, 3548−3553

differences for electron and hole levels, respectively. After another characteristic time $t = t_2$ the band-edge electron−hole pair recombines, emitting a photon of energy $h\nu_1$. During the time interval between t_1 and t_2, electron−phonon coupling is weak enough for carrier transport to be treated within a semiclassical approach using the adiabatic effective mass theory. In contrast, this approach is invalid for transient processes occurring between t_0 and t_1 because the system is in nonadiabatic conditions characterized by strongly coupled carrier and ion dynamics.[25] It is likely that a rich variety of physics in this transient time domain, such as the recently proposed femtosecond-scale insulator−metal transition by ultrafast laser excitation,[26] has yet to be appreciated. The objective of this work is thus to illustrate an example of carrier dynamics in this largely unexplored transient time domain.

Here, we study carrier transport by time-dependent density function theory (TDDFT), coupled with ab initio molecular dynamics. We show that, in the transient time domain, phonon can induce carrier transport. This is to be contrasted with charge transport in the steady-state regime where phonons usually slow down the transport in thermal equilibrium either by electron−phonon scattering or by the formation of polarons that increase the effective mass of the carriers.[27,28] Though the reported effect is expected to be general, we single out surface resonant states (SRSs) because their transport into bulk, according to the semiclassical picture, is strictly forbidden due to the infinitely large perpendicular effective masses m^*. The InAs (110) surface is chosen to illustrate the phonon-mediated coupling between electron states that creates a pathway for localized surface resonant exciton to propagate quickly into the bulk. The phonon-enabled transport process is distinct from other phonon-mediated mechanisms such as superconductivity and dephasing-induced transport.[29−31] We also suggest physical conditions under which this theoretical prediction may be experimentally tested.

To understand real-time nonadiabatic carrier dynamics beyond the Born−Oppenheimer approximation, we employ ab initio molecular dynamics (MD) coupled with the TDDFT formalism,[32] as implemented in the SIESTA code.[33−35] The TDDFT-MD method has recently been applied to adequately describe the electron−ion coupled dynamics.[36−39] We used the norm-conserving Troullier−Martins pseudopotentials,[40] the local density approximation (LDA) for the exchange-correlation functional,[41] and the local basis set of double-ζ polarized orbitals. Though the LDA underestimates the band gap, it provides reasonable band dispersion for InAs surface and bulk states[42] as compared to experiments[43,44] and GW calculation.[45] Also, we found the differences between LDA and GGA functionals are negligibly small in the TDDFT-MD simulation of GeSbTe[46] and graphene.[25] The real-space grid used in the calculations is equivalent to a plane-wave cutoff energy of 100 Ry. The InAs supercell consists of a 16-layer 2 × 2 slab in the [110] direction with 128 atoms per cell. The top surface is 2 × 1 reconstructed,[42] whereas the bottom surface is passivated with hydrogen atoms. The two surfaces are separated by a 15 Å-thick vacuum region to avoid unphysical interactions between periodic images. Γ-point is used to sample the surface Brillouin zone. Ionic positions are fully relaxed before performing the TDDFT simulations with residual forces less than 0.04 eV/Å. We use a time step of 24 attoseconds for the electron dynamics and perform the MD at a temperature of T = 300 K for the ions within the Ehrenfest approximation. The total energy is conserved to within 10^{-4} eV/fs per atom and the variation of the total energy is kept within 0.1 eV.

We will classify the SRSs in Figure 2a into two categories: surface hole states (SHs), whose energy is located approx-

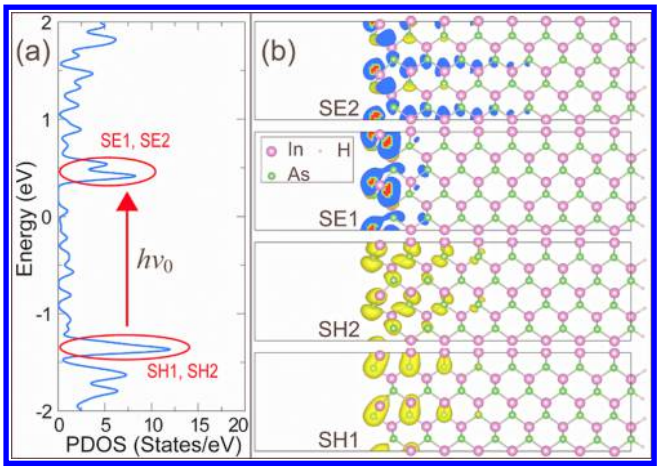

Figure 2. (Color online) Surface resonant states (SRSs) of InAs (110). (a) Projected density of states (PDOS) onto the four-layer atoms near surface with SRSs circled by red. Energy zero is bulk VBM. (b) Corresponding real space charge distributions. The isosurface value is 0.001 e/Å^3.

imately 1.3 eV below the valence band maximum (VBM) and surface electron states (SEs), which lie approximately 0.4 eV above the conduction band minimum. These states are labeled SH1 and SH2 and SE1 and SE2, respectively. The presence of two SHs with a small energy separation, and separately two SEs, is a result of Brillouin zone folding along InAs [1$\bar{1}$0] zigzag chain. Figure 2b shows real-space charge distributions for these states before the excitation. They are all localized on the surface with varying but short decay lengths into the bulk: SH1 and SH2 are bonding states, whereas SE1 and SE2 are antibonding states. Although here we label the excited holes and electrons as SH and SE, they may leave the surface at a later time so the labeling only denotes the initial conditions. At t = 0, we excite the same amount of electrons (0.5 e) from SH1 and SH2 to SE1 and SE2. This setup mimics the actual femtosecond laser excitation with a finite spread of frequencies. In addition, such a choice improves numerical stability in the simulation.

We examine the time evolution of these initially surface-bound states [see Supporting Information (SI)]. To measure the position of the excited particles, we define the center of charge as

$$d_Z^{\mathrm{SRS}}(t) = \int z\rho^{\mathrm{SRS}}(z, t)\mathrm{d}z / \int \rho^{\mathrm{SRS}}(z, t)\mathrm{d}z \quad (1)$$

where the z axis is normal to the surface and $\rho^{\mathrm{SRS}}(z,t)$ is the planar averaged charge of the SRS at position z at time t. As shown in Figure 3a and Figure S1 in SI, it shows that SH1 transfers from surface into bulk: for example, $d_Z^{\mathrm{SH1}}(0\ \mathrm{fs})$ = 3 Å, $d_Z^{\mathrm{SH1}}(24\ \mathrm{fs})$ = 7 Å, and $d_Z^{\mathrm{SH1}}(48\ \mathrm{fs})$ = 9 Å. In a nonpolar surface, there is no measurable electrical field across the slab, so the carrier transport is purely diffusive, as it is driven by the concentration gradient created by the initial excitation. Figure 3a shows $\Delta d_Z^{\mathrm{SRS}}(t) = d_Z^{\mathrm{SRS}}(t) - d_Z^{\mathrm{SRS}}(0)$ for all the four SRSs. It reveals that SH1 has significantly larger transport than any other state. SE2 also exhibits obvious transport, but only after t

DOI: 10.1021/acs.jpclett.6b01608
J. Phys. Chem. Lett. 2016, 7, 3548−3553

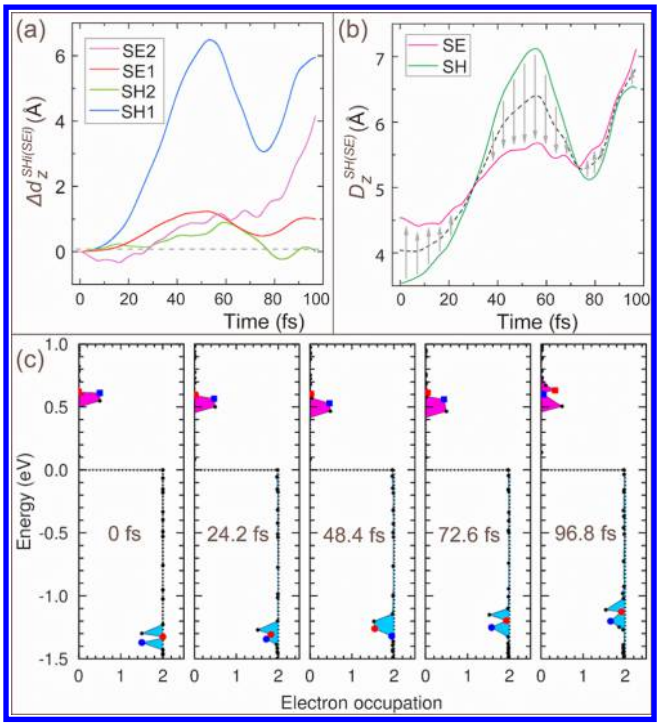

Figure 3. (a) Time evolution of the charge centers $\Delta d_Z^{\mathrm{SH}i(\mathrm{SE}i)}$, where i = 1 and 2. (b) Time evolution of the average positions of the charge centers $D_Z^{\mathrm{SH(SE)}}$. The dashed line denotes the center of electrical dipole, whereas the arrows indicate the instantaneous orientation of the electric field. (c) Change in the electron occupation, which is calculated by projecting the time-evolved wave function onto the eigenstates of the time-independent Hamiltonian. The shaded sky-blue (pink) region stands for hole (electron). The states significantly changing the occupation stand for red and blue dots for hole and boxes for electron.

≥ 80 fs. In contrast, the transport is considerably smaller for SE1 and SH2.

Figure 3b shows the time evolution of the average centers of charge, $D_Z^{\mathrm{SH}} = (d_Z^{\mathrm{SH1}} + d_Z^{\mathrm{SH2}})/2$ for photoexcited holes and $D_Z^{\mathrm{SE}} = (d_Z^{\mathrm{SE1}} + d_Z^{\mathrm{SE2}})/2$ for photoexcited electrons. We see that initially the center of holes, $D_Z^{\mathrm{SH}}(0\ \mathrm{fs})$, is closer to the surface than that of electrons, $D_Z^{\mathrm{SE}}(0\ \mathrm{fs})$. In contrast, at a later time, the transport of the holes, led by SH1, is faster than that of the electrons, with the major contribution from SE2. To understand the charge oscillation, we analyzed the changes in the occupation number for the hole states. It happens that the occupation of the SH1 state [blue dot in Figure 3c] is anticorrelated with that of an adjacent higher-energy bulk state [red dot in Figure 3c] with an oscillation period in close resemblance with the dynamics of the SH1 in Figure 3a. Also, the transport of the SE2 after 80 fs is correlated with the occupation change of the SE2 state [blue box in Figure 3c], which increases one of the adjacent higher energy bulk states [red box in Figure 3c]. Thus, the coupling of SRS with bulk states is the main origin of the transport.

In the semiclassical regime, the group velocity of a carrier is proportional to the first order derivative of the band energy $E(\mathrm{k})$, that is, $\frac{\mathrm{d}E(k)}{\mathrm{d}k}$. Here, however, the velocity for carrier transport is decoupled from this group velocity. In the case of SRSs, for example, the masses in the direction of propagation are infinite and the velocities are zero. Thus, existing semiclassical theories show their limitations and one needs rely on a more complete quantum mechanical theory to account for this phenomenon. To clarify this effect, we plot the time evolution of the energies in Figure 4a, where we notice

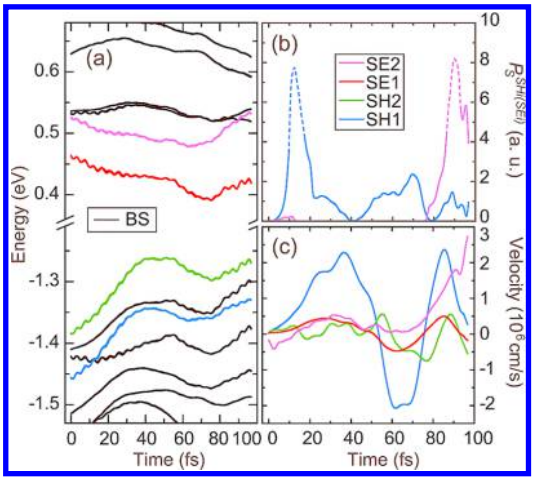

Figure 4. Time evolution of (a) excited state and bulk state (BS) energies and (b) modeled probability P_S. Dashed line indicates regions near singular points in eq 2. For simplicity, in the calculation we assume that the PDOS is nearly constant in the region we considered, that is, $|\varepsilon_s - \varepsilon_b|$ is small. (c) Time evolution of the velocities of centers of charge. Positive (negative) values denote movement into bulk (toward surface).

that significant transport takes place, when the states SH1 and SE2 are close in energy to bulk states. This clearly indicates a phonon-mediated interaction between electronic states: namely, a small change in the atomic positions alters the effective potential experienced by the electrons, which in turn alters the coupling between adjacent electronic energy levels. As a result, the initially surface-bound exciton can eventually diffuse away as delocalized bulk states. Note that, as phonon (or lattice motion)-mediated coupling *between* electronic states is key here, this effect is qualitatively different from the polaron effect where electron−phonon coupling modifies the dispersion of individual electronic states.

To gain further insight into the mechanism driving this phenomenon, we now develop a qualitative model where the phonon-mediated coupling between a propagating state (s) and a bulk state (b) is treated as a phonon emission and absorption process between two electronic states φ_s and φ_b. The transition rate $\mathcal{W}_{sb}$ is treated within the Fermi Golden Rule, that is, $\mathcal{W}_{sb} = \frac{2\pi}{\hbar}|M^2|\delta(\varepsilon_s - \varepsilon_b \pm \hbar\omega_q)$ where $M = \langle\varphi_s|H(t)|\varphi_b\rangle$ is the matrix element of the time-evolving Hamiltonian $H(t)$ between states s and b, ε_s and ε_b are the eigenenergies of the Hamiltonian, and $\hbar\omega_q$ is the phonon energy of momentum q. The coupling strength should also be proportional to the phonon density of states, $\mathrm{PDOS}(\hbar\omega_q)$, and its occupation, $\rho_q = \frac{1}{\exp(\hbar\omega_q / k_B T) - 1}$, where k_B is the Boltzmann constant. The most probable events involve single phonon emission and absorption, namely, $\hbar\omega_q = \varepsilon_s - \varepsilon_b$. Hence, the total probability of the phonon-mediated process is given by the summation over all bulk states

$$P_s = \begin{cases} \frac{2\pi}{\hbar} \sum_{\text{bulk states}} \frac{\mathrm{PDOS}(|\varepsilon_s - \varepsilon_b|)|M^2|}{\exp(|\varepsilon_s - \varepsilon_b|/k_B T) - 1} & \text{if } |\varepsilon_s - \varepsilon_b| \le \hbar\omega_D \\ 0 & \text{if } |\varepsilon_s - \varepsilon_b| > \hbar\omega_D \end{cases} \quad (2)$$

DOI: 10.1021/acs.jpclett.6b01608
J. Phys. Chem. Lett. 2016, 7, 3548−3553

where ω_D is the Debye frequency. Here, we assume that phonon emission rate equals to phonon absorption rate. The effect of spontaneous emission is not considered. Its effect is to increase the slope in Figure 4b, so the qualitative results hold. We approximate the eigen-energies in eq 2 by the time-evolved energies in Figure 4a. As shown in Figure 4b, overall P_S^{SH1} is large, whereas P_S^{SE2} is small initially but increases when t approaches 70 fs. In contrast, P_s's for SE1 and SH2 are negligible, suggesting that for these states higher-order multiphonon processes may dominate.

Figure 4c shows the carrier velocity $V_Z^{SRS}(t)$, defined as the time-derivative of $d_Z^{SRS}(t)$, which may be compared to P_s in Figure 4b. Here, a positive value corresponds to transport into the bulk, whereas a negative value corresponds to transport back toward the surface. Figure 4c reveals that $|V_Z^{SRS}(t)|$ correlates reasonably well with P_S^{SRS}. For example, the velocity of SH1 is typically larger than 2×10^6 cm/s, whereas that of SE2 is less than 0.5×10^6 cm/s, but rapidly increases to 3×10^6 cm/s when t is between 80 and 100 fs. In contrast, the velocities for SE1 and SH2 are around 0.5×10^6 cm/s.

We identify the phonon modes promoting the carrier transport from the energy distribution in phonon modes [see Figure S2 in SI]. It appears that most of the lattice energy is concentrated in the low-frequency modes below 3.5 THz. Among those modes, the 2.6 and 2.7 THz phonons are the most important ones, of which the displacement eigenvectors are localized at the surface.

An important prediction of the model in eq 2 is the temperature dependence of the phonon-mediated coupling, and subsequent transport distance. We have calculated $\Delta d_Z^{SH1}(t)$, in a temperature range between 100 K $\leq T \leq$ 400 K. Figure 5 shows that, in the same amount of time, SH1 moves

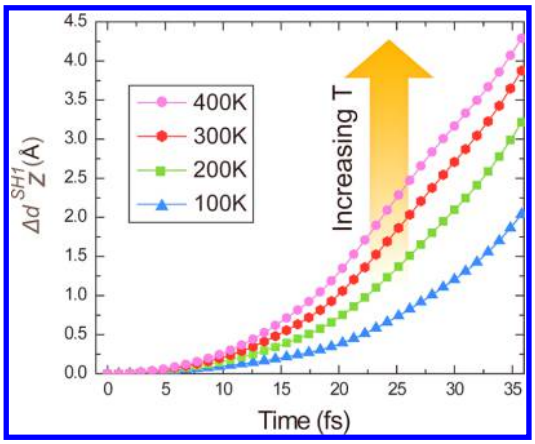

Figure 5. Time evolution of the charge centers Δd_Z^{SH1} in the temperature range from 100 to 400 K, relative to their respective initial positions at $t = 0$.

further into the bulk at an elevated temperature than at a lower temperature, for example, Δd_Z^{SH1} ($t = 35$ fs) is 2 Å at $T = 100$ K, but 4.25 Å at $T = 400$ K. This finding is in clear departure from the current understanding of charge transport because it is conventionally accepted that free-carrier mobility should be reduced by electron−electron and electron−phonon scatterings as temperature increases.[27,28]

The general properties of phonon-enabled carrier transport should be experimentally detectable using femtosecond techniques. In particular, our calculations predict a marked peak in $d(d_Z)/dT$, rather than a monotonic decrease as given by the semiclassical picture. Therefore, at low enough temperature, increasing T could promote carrier transport, until the increased electron−electron and electron−phonon scatterings take over at higher temperature to slow down the process. In addition, similar to ion tunneling in silicon nanocrystals leading to gigahertz emission,[47] here, the nonadiabatic transition between resonant surface and bulk states and the corresponding exciton oscillations can result in an emission, which can be detected in the form of terahertz-frequency radiation. On the basis of Figure 3b, one can estimate the oscillation frequency to be on the order of 10 THz in the nanosize sample, which is nearly ten times larger than the typical frequencies of the photo-Dember effect for InAs surface.[48,49] The difference in the characteristic frequencies reflects the qualitative difference in the transport behavior between the semiclassical and quantum mechanical regimes: though the conventional photo-Dember effect originates from the asymmetry of the electron and hole carrier mobilities, here, it reflects the detailed band structure manifold near the surface. Experimentally, it will be desirable to minimize the bulk region to boost SRS signals from the surface. In this regard, an ultrathin nanostructure might be a better choice.

Recently, a lateral photo-Dember effect was reported for graphene.[15] It is attributed to a mobility asymmetry due to scattering by extrinsic defects. Interestingly, the magnitude of the photocurrent is closely related to hot carrier cooling rate. It hints that phonon-mediated transport may be more pronounced for hot carriers in lower-dimensional systems, and hence, a fully quantum mechanical description becomes necessary. Detecting radiations at unconventional terahertz frequencies in graphene and other two-dimensional systems thus could be another way to confirm our predictions.

In summary, first-principles MD simulation of ion dynamics, coupled with TDDFT for electron dynamics, reveals a transient mechanism in which phonon-mediated coupling between occupied and empty electronic states promotes the transport of excited carriers, in contrast to the typical situation where carrier transport is often slowed down by phonons. Taking the extreme case, SRSs, as a theoretical example, we show that excitations with infinite perpendicular mass can also transfer into bulk with a velocity as high as 10^6 cm/s. The phonon-enabled transport mechanism is not a property unique to the SRSs. Hence, it should also affect the transport when only bulk-like carriers are involved, at least as a higher order effect.

■ ASSOCIATED CONTENT

Supporting Information

The Supporting Information is available free of charge on the ACS Publications website at DOI: 10.1021/acs.jpclett.6b01608.

Time evolution of the charge distribution of SH1 state and the phonon modes of InAs system are contained. (PDF)

■ AUTHOR INFORMATION

Corresponding Authors

*E-mail: jbang0312@kbsi.re.kr.
*E-mail: zhangs9@rpi.edu.

Notes

The authors declare no competing financial interest.

DOI: 10.1021/acs.jpclett.6b01608
J. Phys. Chem. Lett. 2016, 7, 3548−3553

■ ACKNOWLEDGMENTS

S.B.Z. thanks Lawrence Zhang for bringing to our attention the photo-Dember effect. Work at RPI (D.H., J.B., W.Y.X., and S.B.Z.) was supported by the U.S. Department of Energy (DOE) under Grant No. DE-SC0002623. Work at China (D.H.) was supported by the National Natural Science Foundation of China under Grant No. 11504368. Work at Korea (J.B.) was supported by Basic Science Research Program through the National Research Foundation of Korea (NRF) (NRF-2015R1C1A1A02037024) and the National Research Council of Science & Technology grant (No. CAP-16-01-KIST) by the Korea government. V.M. acknowledges a grant from NY Star program. We acknowledge the supercomputer time provided by NERSC under the Grant No. DE-AC02-05CH11231 and the Center of Computational Innovations (CCI) at RPI. We used the VESTA software to generate some of the figures.[50]

■ REFERENCES

(1) Muller, D. A. A Sound Barrier for Silicon? *Nat. Mater.* **2005**, *4*, 645−647.
(2) Muller, D. A.; Sorsch, T.; Moccio, S.; Baumann, F. H.; Evans-Lutterodt, K.; Timp, G. The Electronic Structure at the Atomic Scale of Ultrathin Gate Oxides. *Nature* **1999**, *399*, 758−761.
(3) Heath, J. R.; Ratner, M. A. Molecular Electronics. *Phys. Today* **2003**, *56*, 43.
(4) Nitzan, A.; Ratner, M. A. Electron Transport in Molecular Wire Junctions. *Science* **2003**, *300*, 1384−1389.
(5) Chang, L. L.; Esaki, L.; Tsu, R. Resonant Tunneling in Semiconductor Double Barriers. *Appl. Phys. Lett.* **1974**, *24*, 593.
(6) Britnell, L.; Gorbachev, R. V.; Geim, A. K.; Ponomarenko, L. A.; Mishchenko, A.; Greenaway, M. T.; Fromhold, T. M.; Novoselov, K. S.; Eaves, L. Resonant Tunnelling and Negative Differential Conductance in Graphene Transistors. *Nat. Commun.* **2013**, *4*, 1794.
(7) van Wees, B. J.; van Houten, H.; Beenakker, W. J.; Williamson, J. G.; Kouwenhoven, L. P.; van der Marel, D.; Foxon, C. T. Quantized Conductance of Point Contacts in a Two-Dimensional Electron Gas. *Phys. Rev. Lett.* **1988**, *60*, 848.
(8) Krinner, S.; Stadler, D.; Husmann, D.; Brantut, J.-P.; Esslinger, T. Observation of Quantized Conductance in Neutral Matter. *Nature* **2014**, *517*, 64−67.
(9) Di Ventra, M.; Pantelides, S. T.; Lang, N. D. First-Principles Calculation of Transport Properties of a Molecular Device. *Phys. Rev. Lett.* **2000**, *84*, 979.
(10) Kim, Y. H.; Tahir-Kheli, J.; Schultz, P. A.; Goddard, W. A., III. First-principles Approach to the Charge-Transport Characteristics of Monolayer Molecular-Electronics Devices: Application to Hexanedithiolate Devices. *Phys. Rev. B: Condens. Matter Mater. Phys.* **2006**, *73*, 235419.
(11) Kang, J.; Bang, J.; Ryu, B.; Chang, K. J. Effect of Atomic-Scale Defects on the Low-Energy Electronic Structure of Graphene: Perturbation Theory and Local-Density-Functional Calculations. *Phys. Rev. B: Condens. Matter Mater. Phys.* **2008**, *77*, 115453.
(12) Bang, J.; Chang, K. J. Localization and One-Parameter Scaling in Hydrogenated Graphene. *Phys. Rev. B: Condens. Matter Mater. Phys.* **2010**, *81*, 193412.
(13) Choe, D. H.; Bang, J.; Chang, K. J. Electronic Structure and Transport Properties of Hydrogenated Graphene and Graphene Nanoribbons. *New J. Phys.* **2010**, *12*, 125005.
(14) Shah, J. *Ultrafast Spectroscopy of Semiconductors and Semiconductors Nanostrutures*, 2nd ed.; Springer: Berlin, 1999.
(15) Liu, C.-H.; Chang, Y.-C.; Lee, S.; Zhang, Y.; Zhang, Y.; Norris, T. B.; Zhong, Z. Ultrafast Lateral Photo-Dember Effect in Graphene Induced by Nonequilibrium Hot Carrier Dynamics. *Nano Lett.* **2015**, *15*, 4234−4239.
(16) Fischetti, M. V.; Laux, S. E. Monte Carlo Analysis of Electron Transport in Small Semiconductor Devices including Band-Structure and Space-Charge Effects. *Phys. Rev. B: Condens. Matter Mater. Phys.* **1988**, *38*, 9721−9745.
(17) Fischetti, M. V. Monte Carlo Simulation of Transport in Technologically Significant Semiconductors of the Diamond and Zinc-Blende Structures-Part I: Homogeneous Transport. *IEEE Trans. Electron Devices* **1991**, *38*, 634−649.
(18) Yao, Y.; Si, W.; Hou, X.; Wu, C. Monte Carlo Simulation Based on Dynamic Disorder Model in Organic Semiconductors: From Coherent to Incoherent Transport. *J. Chem. Phys.* **2012**, *136*, 234106.
(19) Gelmont, B.; Kim, K.; Shur, M. Monte Carlo Simulation of Electron Transport in Gallium Nitride. *J. Appl. Phys.* **1993**, *74*, 1818.
(20) Foutz, B. E.; O'Leary, S. K.; Shur, M. S.; Eastman, L. F. Transient Electron Transport in Wurtzite GaN, InN, and AlN. *J. Appl. Phys.* **1999**, *85*, 7727.
(21) O'Leary, S. K.; Foutz, B. E.; Shur, M. S.; Eastman, L. F. Steady-State and Transient Electron Transport within Bulk Wurtzite Zinc Oxide. *Solid State Commun.* **2010**, *150*, 2182−2185.
(22) Johnston, M. B.; Whittaker, D. M.; Corchia, A.; Davies, A. G.; Linfield, E. H. Simulation of Terahertz Generation at Semiconductor Surfaces. *Phys. Rev. B: Condens. Matter Mater. Phys.* **2002**, *65*, 165301.
(23) Su, F. H.; Blanchard, F.; Sharma, G.; Razzari, L.; Ayesheshim, A.; Cocker, T. L.; Titova, L. V.; Ozaki, T.; Kieffer, J.-C.; Morandotti, R.; et al. Terahertz Pulse Induced Intervalley Scattering in Photoexcited GaAs. *Opt. Express* **2009**, *17*, 9620−9629.
(24) Liu, K.; Xu, J.; Yuan, T.; Zhang, X.-C. Terahertz Radiation from InAs Induced by Carrier Diffusion and Drift. *Phys. Rev. B: Condens. Matter Mater. Phys.* **2006**, *73*, 155330.
(25) Bang, J.; Meng, S.; Sun, Y.-Y.; West, D.; Wang, Z.; Gao, F.; Zhang, S. B. Regulating Energy Transfer of Excited Carriers and the Case for Excitation-Induced Hydrogen Dissociation on Hydrogenated Graphene. *Proc. Natl. Acad. Sci. U. S. A.* **2013**, *110*, 908−911.
(26) Wachter, G.; Lemell, C.; Burgdörfer, J.; Sato, S. A.; Tong, X.-M.; Yabana, K. Ab Initio Simulation of Electrical Currents Induced by Ultrafast Laser Excitation of Dielectric Materials. *Phys. Rev. Lett.* **2014**, *113*, 087401.
(27) Yu, P. Y.; Cardona, M. *Fundamentals of Semiconductors: Physics and Material Properties*, 3rd ed.; Springer: New York, 2001; Chapter 5.
(28) Seeger, K. *Semiconductor Physics: An Introduction*, 9th ed.; Springer-Verlag: Berlin, 2004; Chapter 6.
(29) Bardeen, J.; Cooper, L. N.; Schrieffer, J. R. Theory of Superconductivity. *Phys. Rev.* **1957**, *108*, 1175.
(30) Gurvitz, S. A. Delocalization in the Anderson Model due to a Local Measurement. *Phys. Rev. Lett.* **2000**, *85*, 812.
(31) Rebentrost, P.; Mohseni, M.; Kassal, I.; Lloyd, S.; Aspuru-Guzik, A. Environment-Assisted Quantum Transport. *New J. Phys.* **2009**, *11*, 033003.
(32) Runge, E.; Gross, E. K. U. Density-Functional Theory for Time-Dependent Systems. *Phys. Rev. Lett.* **1984**, *52*, 997.
(33) Soler, J. M.; Artacho, E.; Gale, J. D.; García, A.; Junquera, J.; Ordejón, P.; Sánchez-Portal, D. The SIESTA Method for Ab Initio Order-N Materials Simulation. *J. Phys.: Condens. Matter* **2002**, *14*, 2745.
(34) Meng, S.; Kaxiras, E. Real-Time, Local Basis-Set Implementation of Time-Dependent Density Functional Theory for Excited State Dynamics Simulations. *J. Chem. Phys.* **2008**, *129*, 054110.
(35) Sugino, O.; Miyamoto, Y. Density-Functional Approach to Electron Dynamics: Stable Simulation under a Self-Consistent Field. *Phys. Rev. B: Condens. Matter Mater. Phys.* **1999**, *59*, 2579.
(36) Miyamoto, Y.; Zhang, H.; Miyazaki, T.; Rubio, A. Modifying the Interlayer Interaction in Layered Materials with an Intense IR Laser. *Phys. Rev. Lett.* **2015**, *114*, 116102.
(37) Falke, S. M.; Rozzi, C. A.; Brida, D.; Maiuri, M.; Amato, M.; Sommer, E.; De Sio, A.; Rubio, A.; Cerullo, G.; Molinari, E.; et al. Coherent Ultrafast Charge Transfer in an Organic Photovoltaic Blend. *Science* **2014**, *344*, 1001−1005.
(38) Zeb, M. A.; Kohanoff, J.; Sánchez-Portal, D.; Arnau, A.; Juaristi, J. I.; Artacho, E. Electronic Stopping Power in Gold: The Role of d Electrons and the H/He Anomaly. *Phys. Rev. Lett.* **2012**, *108*, 225504.

DOI: 10.1021/acs.jpclett.6b01608
J. Phys. Chem. Lett. 2016, 7, 3548−3553

(39) Meng, S.; Kaxiras, E. Electron and Hole Dynamics in Dye-Sensitized Solar Cells: Influencing Factors and Systematic Trends. *Nano Lett.* **2010**, *10*, 1238−1247.
(40) Troullier, N.; Martins, J. L. Efficient Pseudopotentials for Plane-Wave Calculations. *Phys. Rev. B: Condens. Matter Mater. Phys.* **1991**, *43*, 1993.
(41) Perdew, J. P.; Zunger, A. Self-Interaction Correction to Density-Functional Approximations for Many-Electron Systems. *Phys. Rev. B: Condens. Matter Mater. Phys.* **1981**, *23*, 5048.
(42) Alves, J. L.; Hebenstreit, J.; Scheffler, M. Calculated Atomic Structures and Electronic Properties of GaP, InP, GaAs, and InAs(110) Surfaces. *Phys. Rev. B: Condens. Matter Mater. Phys.* **1991**, *44*, 6188−6198.
(43) Swanston, D. M.; Mclean, A. B.; McIlroy, D. N.; Heskett, D.; Ludeke, R.; Munekata, H.; Prietsch, M.; DiNardo, N. J. Surface Localized States on InAs(110). *Surf. Sci.* **1994**, *312*, 361−368.
(44) Andersson, C. B. M.; Andersen, J. N.; Persson, P. E. S.; Karlsson, U. O. Bulk and Surface Electronic Structure of InAs(110). *Surf. Sci.* **1998**, *398*, 395−406.
(45) López-Lozano, X.; Pulci, O.; Noguez, C.; Fleischer, K.; Del Sole, R.; Richter, W. Electronic Structure and Reflectance Anisotropy Spectrum of InAs(110). *Phys. Rev. B: Condens. Matter Mater. Phys.* **2005**, *71*, 125337.
(46) Bang, J.; Sun, Y. Y.; Liu, X.-Q.; Gao, F.; Zhang, S. B. Non-Thermal Phase Transition beyond the Steady-State Approximation. 2016, *arXiv: 1601.04387*. arXiv.org e-Print archive. https://arxiv.org/ftp/arxiv/papers/1601/1601.04387.pdf (accessed July 15 2016).
(47) Vach, H. Terahertz and Gigahertz Emission from an All-Silicon Nanocrystal. *Phys. Rev. Lett.* **2014**, *112*, 197401.
(48) Gu, P.; Tani, M.; Kono, S.; Sakai, K.; Zhang, X.-C. Study of Terahertz Radiation from InAs and InSb. *J. Appl. Phys.* **2002**, *91*, 5533.
(49) Seletskiy, D. V.; Hasselbeck, M. P.; Cederberg, J. G.; Katzenmeyer, A.; Toimil-Molares, M. E.; Léonard, F.; Talin, A. A.; Sheik-Bahae, M. Efficient Terahertz Emission from InAs Nanowires. *Phys. Rev. B: Condens. Matter Mater. Phys.* **2011**, *84*, 115421.
(50) Momma, K.; Izumi, F. VESTA 3 for Three-Dimensional Visualization of Crystal, Volumetric and Morphology Data. *J. Appl. Crystallogr.* **2011**, *44*, 1272−1276.

DOI: 10.1021/acs.jpclett.6b01608
J. Phys. Chem. Lett. 2016, 7, 3548−3553